

# Dimerization of European Robin Cryptochrome 4a

Maja Hanić,<sup>♦</sup> Lewis M. Antill,<sup>♦</sup> Angela S. Gehrckens,<sup>♦</sup> Jessica Schmidt, Katharina Görtemaker, Rabea Bartölke, Tarick J. El-Baba, Jingjing Xu, Karl-Wilhelm Koch, Henrik Mouritsen, Justin L. P. Benesch, P. J. Hore, and Ilia A. Solov'yov\*



Cite This: *J. Phys. Chem. B* 2023, 127, 6251–6264



Read Online

ACCESS |



Metrics & More

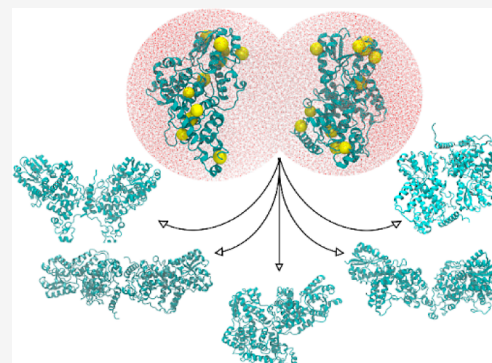


Article Recommendations



Supporting Information

**ABSTRACT:** Homo-dimer formation is important for the function of many proteins. Although dimeric forms of cryptochromes (Cry) have been found by crystallography and were recently observed in vitro for European robin Cry4a, little is known about the dimerization of avian Crys and the role it could play in the mechanism of magnetic sensing in migratory birds. Here, we present a combined experimental and computational investigation of the dimerization of robin Cry4a resulting from covalent and non-covalent interactions. Experimental studies using native mass spectrometry, mass spectrometric analysis of disulfide bonds, chemical cross-linking, and photometric measurements show that disulfide-linked dimers are routinely formed, that their formation is promoted by exposure to blue light, and that the most likely cysteines are C317 and C412. Computational modeling and molecular dynamics simulations were used to generate and assess a number of possible dimer structures. The relevance of these findings to the proposed role of Cry4a in avian magnetoreception is discussed.



## INTRODUCTION

Oligomerization of proteins can change their structural stability, activity, and mechanisms of action<sup>1,2</sup> and is important in numerous processes in living organisms. Examples from the cryptochrome (Cry) protein family include a tetrameric structure of *Arabidopsis thaliana* Cry2 (AtCry2) important in photoactivation,<sup>3</sup> a proposed dimer of L-Cry involved in the reproduction cycle of the bristle worm, *Platynereis dumerilii*,<sup>4</sup> and dimerization of AtCry1.<sup>5,6</sup>

In the investigation reported here, we focus on Cry, a protein found in all biological kingdoms.<sup>7–12</sup> Crys are structurally similar to light-activated DNA photolyases<sup>7,12,13</sup> and consist of two main structural regions: a highly conserved N-terminal photolyase homology region (PHR) and the intrinsically disordered C-terminal tail (CTT).<sup>14</sup> Most Crys have a flavin adenine dinucleotide cofactor (FAD) that absorbs UV-blue light, non-covalently bound in the PHR domain.<sup>7</sup> Crys can exist in the so-called dark-state, containing the fully oxidized form of the FAD, or in higher energy states formed by photo-excitation of the FAD followed by the formation of radical pairs, involving a triad or tetrad of tryptophan residues, which have been proposed as mediators of the mechanism of magnetoreception in migratory songbirds.<sup>15–20</sup> Three different Cry-genes, Cry1,<sup>21–26</sup> Cry2,<sup>21,27</sup> and Cry4<sup>28–32</sup> exist in most bird species, each with at least one splice-variant.<sup>22,33,34</sup> Several of these Crys are found in the birds' retinas, where they can easily be light-activated.<sup>21,24,25,27,29,32,34</sup> Light-activated Cry is believed to form a signaling state, via a conformational change in the CTT, which has been the subject of computational

studies of European robin Cry4a (*Erithacus rubecula*, ErCry4a)<sup>35</sup> and pigeon Cry4a (*Columba livia*, ClCry4a)<sup>36</sup> and experimental investigations of Crys from the fruit fly (*Drosophila melanogaster*, DmCry),<sup>37</sup> chicken (*Gallus gallus*, GgCry4a),<sup>38</sup> and *Arabidopsis* (AtCry1).<sup>39</sup> The exact process by which Cry combines photo-excitation with detection of the Earth's magnetic field to form a long-lived signaling state is unknown but could conceivably involve dimerization. The importance of homo-oligomerization of plant Crys in vivo is clear<sup>40,41</sup> and optogenetic studies of AtCry2 show that the full-length protein undergoes light-induced oligomerization and that functionality is lost in a truncated form that lacks the CTT domain.<sup>42</sup>

For a signal transduction cascade to function, Cry must interact with other proteins. Wu et al. recently listed six proteins as candidate ErCry4a interaction partners.<sup>43</sup> A subsequent detailed biochemical investigation of ErCry4a and a cone-specific G-protein from European robin demonstrated that these two proteins interact directly with each other.<sup>44</sup> Dimers of ErCry4a have also been reported,<sup>15</sup> but it is unclear whether/how a monomer–dimer equilibrium might be

**Received:** February 25, 2023

**Revised:** May 16, 2023

**Published:** July 10, 2023



involved in the downstream signaling process. Within the Cry family there are reports of crystallographic dimeric asymmetric units, including *DmCry*<sup>45</sup> and mouse (*Mus musculus*) *MmCry1* and *MmCry2*<sup>46</sup> (Figure 1). A study of full-length *DmCry* noted

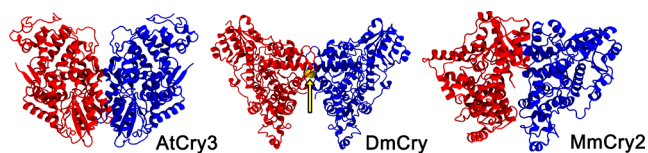


**Figure 1.** Structures of Cry dimers from the Protein Data Bank (PDB): non-covalent AtCry3 dimer (PDB: 2J4D),<sup>3</sup> covalent *DmCry* dimer (PDB: 4GU5)<sup>28</sup> (the arrow indicates the C296–C296 disulfide bond), and non-covalent *MmCry2* dimer (PDB: 6KX8).<sup>29</sup>

an intermonomer disulfide bond, but deemed it to be an artifact of the crystallization method.<sup>47</sup> To date, there has been little work on the dimers of animal Crys, and their function, if any, is unknown.

To learn more about *ErCry4a* dimerization and its possible role in magnetoreception,<sup>15,18</sup> we have explored a variety of candidate structures, including covalently and non-covalently linked forms of the full-length and truncated protein, using a combination of experimental and computational methods to identify potential *ErCry4a* dimers. Native mass spectrometry (MS), mass photometry (MP), and gel electrophoresis of wild-type (WT) and mutant proteins were used to establish the presence and nature of the dimers, while chemical cross-linking followed by MS (XL-MS) provided information about the relative orientation of the monomer units. A combination of molecular docking and molecular dynamics (MD) techniques provided model structures for comparison with the experimental data.

## METHODS

**Experimental Methods. Protein Expression and Purification.** WT *ErCry4a* (GenBank: KX890129.1) was cloned, expressed, and purified as described by Xu et al.<sup>15</sup> with the following modifications. The LB media contained 10 g L<sup>-1</sup> yeast extract, and the expression time was 44 h instead of 22 h. The mutants were generated using the Q5 site-directed mutagenesis kit (New England Biolabs, Ipswich, MA, USA), and plasmids were confirmed by Sanger sequencing (LGC Genomics). For the C412A mutant and the 5-cysteine mutant (C68A + C73A + C116A + C189A + C317A), an *E. coli* K12 codon-optimized version of *ErCry4a* was used, generated by Eurofins Genomics (Ebersberg, Germany). Tables 1 and 2 summarize the primers used for each mutation. Mutant proteins were expressed and purified in the same way as the WT protein with the following exception: double, triple, and 5-cysteine mutants were expressed in BL21-CodonPlus(DE3)-RIPL *E. coli* cells (Agilent, Santa Clara, CA, USA) in the dark, starting with a 30 mL culture grown overnight at 30 °C and 250 rpm, a preculture inoculated to an OD<sub>600</sub> of 0.05 for 6–

6.5 h at 37 °C, and a main culture inoculated with the preculture to an OD<sub>600</sub> of 0.5 for about 3 h at 37 °C until the OD<sub>600</sub> reached 0.6, when the shakers were set to 15 °C and 160 rpm. After about 45 min, at an OD<sub>600</sub> of 0.9 to 1.0, protein expression was induced with 5 μM isopropyl β-D-1-thiogalactopyranoside. Cell harvest, lysis, and purification using Ni-NTA agarose columns and anion exchange chromatography were all performed as described in Xu et al.<sup>15</sup> Purified protein samples were either used directly for photometric cysteine exposure measurements or buffer-exchanged, to remove reducing agents, into 20 mM Tris, pH 8.0, 250 mM NaCl, and 20% glycerol using Sephadex G 25 in PD10 desalting columns (Cytiva, Uppsala, Sweden). The protein samples for XL-MS were produced in insect cells essentially as described previously<sup>44</sup> with the additional step of removing the His-tag. To cleave the His-tag from the Ni-NTA eluted protein, the samples were buffer-exchanged into 20 mM Tris, pH 8.0, 100 mM NaCl, 2 mM DL-dithiothreitol (DTT), using Sephadex G 25 in PD10 desalting columns (Cytiva), and the His-tag was cut off overnight at 4–9 °C by the addition of 10 U AcTEV protease (Thermo Fisher). *ErCry4a* was further purified using anion-exchange chromatography as previously described.<sup>44</sup> All purified protein samples were concentrated to ~3.5 mg mL<sup>-1</sup>. The samples were snap-frozen in liquid nitrogen and stored at –80 °C until shipment to Oxford on dry ice.

**Native Mass Spectrometry and SDS–PAGE.** Native MS and sodium dodecyl sulfate–polyacrylamide gel electrophoresis (SDS–PAGE) were used to investigate the dimeric nature of *ErCry4a*. The *ErCry4a* samples used for these experiments were shipped overnight to Oxford on dry ice from the production laboratory at the University of Oldenburg, in a buffer containing 20 mM Tris, 250 mM NaCl, and 20% glycerol at pH 8. The samples were kept at –80 °C until they were thawed on ice and buffer-exchanged into 200 mM ammonium acetate, pH 8, for the native MS measurements using Zeba Micro Spin desalting columns with a molecular weight exclusion limit of 40 kDa (Thermo Fisher Scientific). All samples included an N-terminal 10× His-tag used for purification of the proteins.

Measurements were performed in Oxford using in-house gold-plated capillaries on a Q Exactive mass spectrometer in positive ion mode. The samples were sprayed using nanoflow electrospray with a source temperature of 150 °C and a capillary voltage of 1.0 kV.<sup>48</sup> The higher-energy C-trap dissociation (HCD) cell voltage was 5 V, in-source trapping was set to –200 V to help with the dissociation of small ion adducts, and the noise threshold parameter was 3. Ion transfer optics and voltage gradients throughout the instruments were adjusted for optimum protein transmission.

For SDS–PAGE gels, the samples were kept covered in the dark or subjected to blue light (450 nm, ~0.3 mW) for 20 min at room temperature at a concentration of ~8 μM. 3.2 μg of each sample were then mixed with diluted NuPAGE LDS

**Table 1. Mutations Introduced in Non-Codon-Optimized *ErCry4a***

mutation	forward primer	reverse primer
C116A	CAACATCCAGGCCCTGGGGGCGAG	GCCTCCATCTCCTTGTAATAATG
C313A	GAACCCCATCGCCCTCCAGATCTGC	CCAGCCATCTGGGTGAAG
C317A	CCTCCAGATCGCCTGGTACAAGGATGCAG	CAGATGGGGTTCAGCC
C313A + C317A	GATCGCCTGGTACAAGGATGCAGAG	TGGAGGGCGATGGGGTTCAGCCAT

**Table 2. Mutations Introduced in Codon-Optimized *ErCry4a***

mutation	forward primer	reverse primer
C68A + C73A	GGATCGGCCCTGCTTGTGATTCAGGGTG	AAGCTGGGCCAGGTTCTTATGCAGATCC
C116A	GAACATTCAGGCCTTGGGTGCAG	GCCTCCATCTCCTTGTAG
C189A	TCTTGCCGAAGCCTATCGTGTTCGGTTAC	TCCGGATCTGGAGCCGAA
C317A	TCTGCAGATTGCCTGGTATAAAGACGCAGAAC	CAGATCGGATTGCCCGCC
C412A	CCGGATTTTCGCCCTGTACGCTTTG	GTGTACTGGTGAAGAAGG

sample buffer (4X) (Invitrogen, Waltham, MA, USA) before being loaded on NuPAGE Novex 4–12% bis-Tris gels, 1.0 mm × 10 well (Invitrogen) and run with NuPAGE MES SDS running buffer (20X) (Invitrogen). The samples of proteins without a His-tag, containing 2 mM DTT (Sigma-Aldrich), were shipped to Oxford and kept in the light while being incubated with different concentrations of DTT for 20 min at room temperature prior to being submitted to the SDS–PAGE gel. Protein bands were visualized by Coomassie blue staining using QuickBlue Protein Stain (LuBio, Zürich, Switzerland) and accompanied by either a SeeBlue Plus2 Pre-stained Protein Ladder (Invitrogen) or a PageRuler Prestained Protein Ladder (Thermo Scientific, Waltham, MA, USA). The software GelAnalyzer 19.1<sup>49</sup> was used for evaluation of the gel bands.

**Mass Photometry.** All samples were shipped as described above except for the *ErCry4a* WT sample used in Figure 3, which was shipped with the addition of 2 mM DTT to limit higher order oligomerization during shipping. This sample was diluted to a concentration of ~44 nM in 200 mM ammonium acetate, pH 8.3, prior to measurement. All other samples were buffer-exchanged into 200 mM ammonium acetate, pH 8.0, and diluted to 13–15 nM. MP measurements were performed essentially as described previously (Young et al.<sup>50</sup>), on a ONE<sup>MP</sup> instrument (Refeyn Ltd, Oxford) in the case of the *ErCry4a* WT sample in Figure 3 and on a TWO<sup>MP</sup> instrument (Refeyn Ltd, Oxford) in all other cases. Briefly, a borosilicate microscope coverslip (Thorlabs) was cleaned by ultrasonication for 5 min in a 1:1 mix of ultrapure water and isopropanol followed by another 5 min of ultra-sonication in ultrapure water and then dried under a stream of nitrogen. Cleaned coverslips and Grace Bio-Labs reusable CultureWell gaskets (Bio-Labs) were assembled into flow chambers. 10–20  $\mu$ L of the sample was added to the flow chamber and images of a  $3.5 \times 12.2 \mu\text{m}^2$  region of the glass coverslip surface were acquired at 1000 frames  $\text{s}^{-1}$ . The mass distributions were obtained from contrasts of ratiometric data by calibration using DiscoverMP (Refeyn Ltd, Oxford).

**Mass Spectrometric Analysis of Chemically Cross-Linked Peptides.** XL-MS was used to probe the interaction surfaces of the linked monomers. The samples for XL-MS were sent to Oxford as described above, with the addition of 2 mM DTT in the shipping buffer to limit higher-order oligomerization. Furthermore, His-tags were cut leaving only five additional amino acids at the N-terminus (GAMGS).

To investigate potential disulfide bonds, protein solutions were incubated with the linkers disuccinimidyl sulfoxide (DSSO)<sup>51</sup> or disuccinimidyl dibutyric acid (DSBU)<sup>52</sup> to cross-link primary amines at the dimer interface using the manufacturer's recommended procedure, as described previously.<sup>53</sup> Cross-linked and non-cross-linked proteins were resolved using SDS–PAGE for analysis of the cross-linkers and direct analysis of the disulfide bonds.

Bands were excised from gels and prepared for MS as described by Shevchenko et al.<sup>54</sup> After in-gel digestion, peptides were resolubilized in buffer A ( $\text{H}_2\text{O}$ , 0.1% formic acid), and ~5–10  $\mu$ L of peptide was loaded onto a reverse-phase trap column (Acclaim PepMap 100, 75  $\mu\text{m} \times 2 \text{ cm}$ , NanoViper, C18, 3  $\mu\text{m}$ , 100 Å, Thermo Fisher, Waltham, MA, USA) using an Ultimate 3000 autosampler and washed with 40  $\mu$ L of buffer A at a flow rate of 20  $\mu\text{L min}^{-1}$ . The trapped peptides were then separated by applying a 15 cm reverse-phase analytical column (Acclaim PepMap 100 C18, 3  $\mu\text{m}$ , 150 mm × 0.075 mm) using a 105 min linear gradient from 5 to 55% buffer B (80% acetonitrile, 20% water, 0.1% formic acid) at a flow rate of 300 nL  $\text{min}^{-1}$ . Long and hydrophobic peptides were washed from the column using 99% buffer B for 15 min at the same flow rate. The separated peptides were electrosprayed in the positive ion mode into an Orbitrap Eclipse Tribrid mass spectrometer (Thermo Fisher) operated in data-dependent acquisition mode (3 s cycle time) using the workflow recommended by the DSSO and DSBU methods programed by the manufacturer. Briefly, precursor scans were collected in the Orbitrap analyzer at 60,000 resolving power at  $m/z$  200 with a mass range of 375–1600  $m/z$ . The precursors above the intensity threshold of  $1.0 \times 10^4$  having charge states between  $z = 4$  and  $z = 8$  were isolated using the quadrupole (0.5  $m/z$  offset, 1.6  $m/z$  isolation window) and fragmented in the linear ion trap using collision-induced dissociation (collision energy = 25%). Peptide fragments were analyzed using the Orbitrap at a resolving power of 30,000 at  $m/z$  200 with a maximum injection time of 70 ms. Fragment ions with  $z = 2$  to  $z = 6$  spaced by the targeted mass difference of 25.9 or 31.9 Da ( $\pm 10$  ppm) corresponding to peptides cross-linked by DSBU or DSSO, respectively, were subjected to further sequencing in the linear ion trap operated in rapid detection mode (35% collision energy, MS1 isolation of 2.5  $m/z$  and MS2 isolation of 2.6  $m/z$ ). Additional MS/MS scans for the precursors within 10 ppm were dynamically excluded for 30 s following the initial selection. The cross-linking data were analyzed using the free software tool MeroX<sup>55</sup> available at [www.StavroX.com](http://www.StavroX.com).

**Cysteine Exposure Measurements.** Quantitative determination of thiol groups in solution was achieved essentially as described previously<sup>56</sup> by recording the formation of 5-thio-2-nitrobenzoic acid (TNB) from 5,5'-dithio-bis-(2-nitrobenzoic acid) (DTNB) at a wavelength of 412 nm. Briefly, WT *ErCry4a*, mutants C317A, C412A, and the 5-cysteine mutant were dialyzed overnight in 100 mM Tris/HCl at pH 8.0. Next, a fresh 12 mM DTNB solution in 100 mM Tris/HCl, pH 8.0, was produced. A calibration curve with 0, 5, 10, 15, 20, 25, and 30  $\mu\text{M}$  L-cysteine and 60  $\mu\text{M}$  DTNB was prepared to calculate the slope of the line (see Figure S3). After adding DTNB, the samples were incubated for 10 min at room temperature. Afterwards, the absorbance of TNB in the Cry samples was measured at 412 nm. To measure the accessibility of cysteines in the proteins, 5  $\mu\text{M}$  of WT *ErCry4a* and of the *ErCry4a* mutants were incubated for 10 min at room temperature with



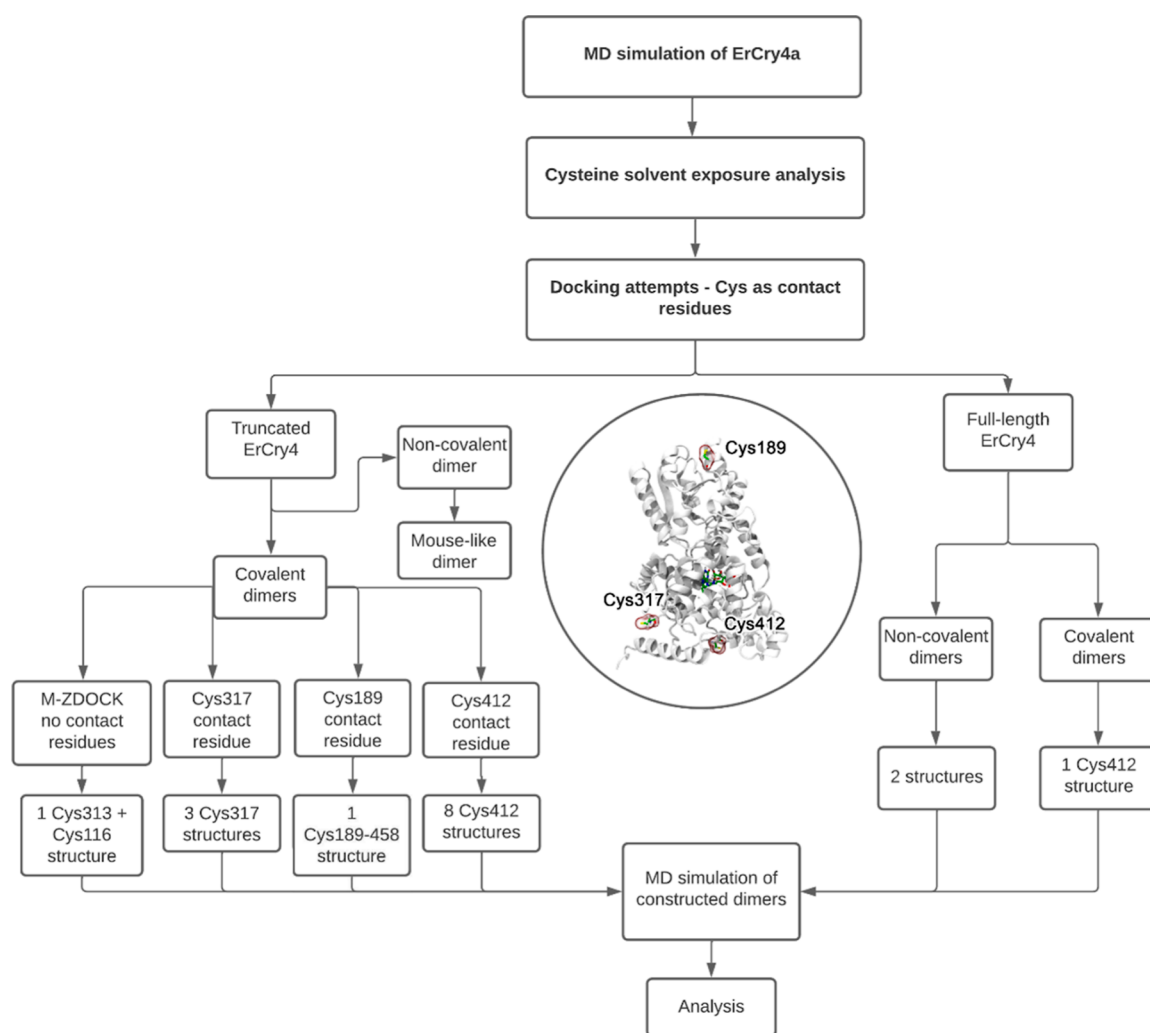


**Figure 2.** Computational workflow used to produce the 16 dimeric structures of *ErCry4a*. The inset in the middle highlights the contact cysteine residues (C317, C412, and C189) which were used in constructing the covalent dimers. An overview of all structures obtained during the docking procedure can be found in the Supporting Information in Tables S10–S18.

60  $\mu\text{M}$  DTNB in 100 mM Tris/HCl at pH 8.0. The number of accessible cysteines was calculated using the expression,  $N_{\text{Cys}} = E/ac$ , where  $E$  is the total absorbance of the sample,  $a$  is the slope of the calibration graph, and  $c$  is the concentration of protein in the solution. All measurements were done under ambient light conditions.

**Computational Methods.** Dimer formation through both covalent and non-covalent interactions of surface residues has been investigated for both full-length and truncated *ErCry4a* structures. All of the dimers studied were classified into families representing groups of structures according to the type of interaction, i.e., covalent (cov) or non-covalent (ncov). The covalent structures were labeled  $\text{cov}(N)^n$ , where  $N$  is the sequence number of the cysteine residue in the monomer subunits that forms the disulfide bond and  $n$  labels a particular dimer within the family. Additionally, some dimer names were abbreviated using the form  $\text{cov}^{\text{NA}}$  or  $\text{cov}^{\text{NB}}$  (e.g., see Table S9).

**Identifying Exposed Residues for Covalent Dimer Construction.** Covalently linked dimers arise from the formation of disulfide bonds between cysteine residues. Figure 2 summarizes the overall workflow for constructing the 16 *ErCry4a* dimeric structures we have investigated. A previously simulated *ErCry4a* construct, including the FAD cofactor, was

used for an analysis of the solvent exposure of the 11 cysteines in *ErCry4a*.<sup>15</sup> 50 snapshots, taken from a 200 ns MD simulation, were time-averaged and evaluated using GETAREA2.<sup>57</sup> To compare solvent-accessible surface area (SASA) values for different amino acids, the absolute SASA for each residue<sup>58</sup> was divided by the maximum SASA (MSA) value for the corresponding amino acid (X) in a Gly–X–Gly tripeptide. A similar method was introduced in earlier work.<sup>59</sup> Gly–X–Gly tripeptides were constructed with Pep McConst software and simulated for 1 ns in a waterbox using NAMD. MSA values for the X residues were determined using GETAREA2.<sup>57</sup> The solvent exposure for residue,  $i$ , was calculated as

$$S_i = \frac{\text{SASA}_i}{\text{MSA}_i} \times 100\% \quad (1)$$

**Covalent Dimer Construction.** The ZDOCK docking tool<sup>61–63</sup> was used to create a set of *ErCry4a* dimers using the seven most solvent-exposed cysteine residues as the docking sites (Table 3). ZDOCK allows one to define a contact residue for dimer construction such that the defined residues in the monomers are placed in close proximity to each other. For the six most solvent-exposed cysteine residues



**Table 3. Summary of *ErCry4a* Dimer Structures Produced by ZDOCK and M-ZDOCK and the MD Simulations<sup>a</sup>**

contact residues	docked structures	simulated structures	simulation time (ns)
covalent dimeric structures			
68	10	0	
73	10	0	
116	10	0	
179	10	0	
189	3	1	100
317	3	3	400
412	3	8	150
none	10	1	100
none (M-ZDOCK)	10	1	100
non-covalent dimeric structures			
none	10	2	400

<sup>a</sup>The specified lengths of the simulations apply to each member of the protein family.

(C68, C73, C116, C189, C317, and C412) together with C179, 49 dimeric structures were constructed, and inter-cysteine distances were analyzed to determine the possibility of disulfide bond formation (see Tables S10–S18). Docking of two *ErCry4a* monomers with the contact residues Cys68 (Table S10), Cys73 (Table S11), Cys116 (Table S12), or Cys179 (Table S13) produced 10 dimeric structures. However, because the cysteine residues were more than 10 Å apart, these structures were not considered in the MD simulations (Table S19). With Cys189 (Table S14) and Cys317 (Table S15) as contact residues, four dimers were found in which one and three structures, respectively, contained the cysteines in close enough contact to warrant proceeding to MD simulations. The disulfide bonds were introduced with NAMD<sup>64</sup> by removing the hydrogen atoms from the cysteine SH groups and defining an abnormally long covalent connection between the sulfur atoms. During the follow-up equilibration, the bond acquired the length of a typical disulfide bond causing a slight rearrangement of atoms at the interface to accommodate the structural change. With Cys412 as the contact residue, ZDOCK yielded three dimeric structures (Table S16) in which the cysteines were somewhat separated, making them unstable in short MD simulations. Because the experimental results (below) suggested that the Cys412 residue was potentially important for dimerization, we have used snapshots from the short MD simulation to construct and simulate eight dimeric configurations for the Cys412 family by first imposing an artificial constraint on the Cys412–Cys412 bond to help the residues move closer together and then removing the constraint.

An additional 10 structures were generated without explicitly specifying a contact residue (Table S17). Furthermore, the M-ZDOCK tool<sup>65</sup> was used to search for different plausible *ErCry4a* dimer structures by predicting cyclically symmetric multimers based on the structure of the *ErCry4a* monomer (Table S18). In the case of a dimer, ten symmetric structures were obtained, but only one, referred to as cov<sup>D</sup>, was analyzed further (Table S18). This dimer contained two disulfide bonds: C116–C313 and C313–C116.

**Non-Covalent Dimer Construction.** The computational tool I-TASSER<sup>66–69</sup> was used to generate the intrinsically disordered CTT (residues 498–527) missing from the crystal structure of pigeon *Cry4a* (PDB code: 6PU0)<sup>28</sup> to obtain a

full-length (FL) homology model, *ErCry4aFL*, with a (confidence) C-score of 0.34. This parameter reports the quality of the predicted model and ranges from −5 to +2, where a higher value signifies a model with a higher confidence (Table S5). The C-score is calculated based on the significance of threading template alignments with subsequent reassembly using replica-exchanged Monte Carlo simulations and the convergence parameters of the structure assembly simulations.<sup>66–69</sup>

Structures of possible *ErCry4aFL* non-covalently bound dimers were generated using ZDOCK.<sup>61</sup> Shape complementarity was taken into consideration, where the algorithm keeps one monomer fixed and rotates and translates the other to find configurations that result in the best fitting score. In the investigation of possible covalent and non-covalent dimers, ZDOCK produced 2000 dimer configurations, of which the top 10 were used for further investigation. These 10 structures were chosen using an energy-based scoring function which includes the potential energy, spatial complementarity, and electric field force between the protein subunits.

**Dimeric Structure Inspired by *MmCry2*.** Dimer interfaces have a high degree of conservation in evolutionarily related proteins.<sup>1</sup> Even though the crystallographic dimer of *MmCry2* has not been identified as being functionally relevant, it is still the closest protein to *ErCry4a* for which a dimer crystal structure has been reported (PDB: 6KX8).<sup>46</sup> A dimeric structure inspired by *MmCry2* was thus constructed, in which the monomers were structurally aligned with the *MmCry2* dimer subunits.

**Molecular Dynamics Simulations.** All MD simulations were conducted using the NAMD package<sup>64,70</sup> through the VIKING platform.<sup>71</sup> The CHARMM36 force field included CMAP corrections for proteins<sup>72,73</sup> and additional parameterizations for FAD.<sup>29,74–76</sup> Periodic boundary conditions were adopted in all MD simulations, and the particle mesh Ewald summation method was employed to evaluate long-range Coulomb interactions. Van der Waals interactions were treated using a smooth cut-off of 12 Å with a switching distance of 10 Å. The simulation temperature was 310 K, controlled with the Langevin thermostat.<sup>70</sup> A constant pressure of 1 atm for equilibrium simulations was obtained using the Langevin piston Nosé–Hoover method.<sup>77</sup> The SHAKE algorithm was used to constrain bonds including hydrogen atoms at their respective equilibrium distances. After 10,000 NAMD<sup>70</sup> minimization steps, harmonic restraints were initiated in the system and gradually released to achieve an equilibrium structure. Equilibration simulations were conducted with explicit solvent modeled through the TIP3P parameter set,<sup>78</sup> with water molecules surrounding the dimers to a distance of 15 Å in all directions. A NaCl salt concentration of 50 mM was assumed in all simulations. After the equilibration, production simulations with temperature control (310 K) within the NVT statistical ensembles were performed (Table S19). All MD simulation results were analyzed with VMD.<sup>79</sup>

## RESULTS AND DISCUSSION

We have studied the dimerization of *ErCry4a* using experimental and computational approaches in parallel. Computational results have been used to guide the experiments and vice versa at various stages of the investigation.

***ErCry4a* Forms a Population of Disulfide-Linked Dimers.** Figure 3A shows a native mass spectrum of WT *ErCry4a*. Two charge-state series consistent with the monomer

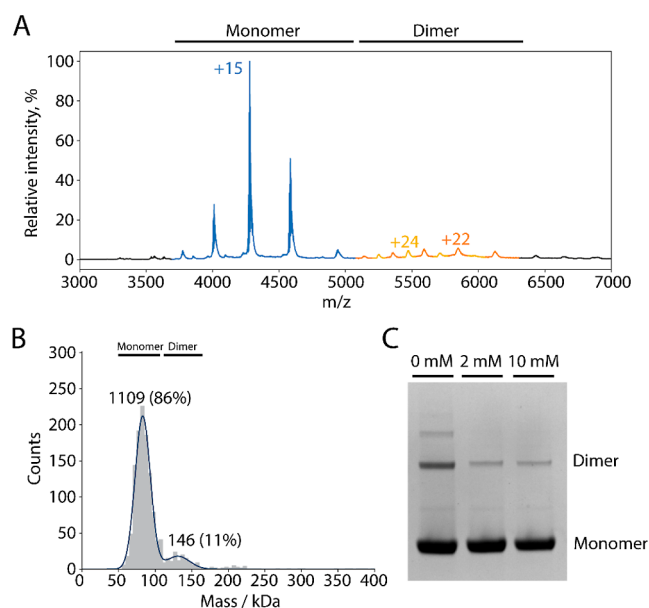


**Figure 3.** (A) Native mass spectrum of *ErCry4a*. The peaks of the monomer region are indicated in blue (molecular mass  $64.197 \pm 0.029$  kDa) and the peaks of the dimer region in orange and yellow (molecular masses  $\sim 123$  and  $\sim 131$  kDa). The expected mass of an *ErCry4a* WT monomer including FAD and a His-tag is 64.034 kDa. The differences between the detected and the expected masses are due to salt ions and buffer components. The finding of a second dimer mass, lower than the expected mass, could be due to minor truncations and is only observed in some samples. The observation here of stable dimers is consistent with Figure S13 of Xu et al.<sup>15</sup> The sample used for this measurement contained 10 mM  $\beta$ -mercaptoethanol (BME) during shipment to prevent higher order oligomerization. (B) MP of 44 nM *ErCry4a*. The same sample as in (A) but shipped with 2 mM DTT. The numbers above the peaks are the numbers of counts. (C) SDS–PAGE gel of the *ErCry4a* samples without a His-tag (the same as used for XL-MS) that had been incubated with various amounts of DTT.

and dimer can be seen: major peaks correspond to the monomer, and minor peaks in the range  $m/z = 5000$ – $7000$  to the dimer.

To investigate the dimerization further, WT *ErCry4a* was studied by MP (Figure 3B). Two peaks were observed, a major component (60–80 kDa, 86%) from monomers and a minor component (120–160 kDa, 11%) attributed to dimers. The observation of dimeric forms of *ErCry4a* both by native MS (at micromolar protein concentrations) and MP (at nanomolar

concentrations) suggests that the two monomer units are strongly bound and not an artifact of nanoelectrospray ionization. Non-specific, non-covalent dimers would be expected to dissociate at high dilution. Notably, the relative abundance of dimers and monomers was the same in both the MS and MP experiments despite the large difference in sample concentration, suggesting that the dimers are covalently linked. To test this possibility, we ran SDS–PAGE gels of the *ErCry4a* samples after incubation with various concentrations of the DTT reductant (Figure 3C). Bands from dimers and higher order oligomers, visible under the denaturing conditions of the gels in the absence of DTT, are attenuated by DTT-treatment, consistent with dimer formation via covalent inter-monomer disulfide bonds. The complete gel is shown in Figure S1.

**Cysteine Solvent-Accessibility Calculations.** On the basis that the covalent links responsible for dimerization are most likely to be disulfide bonds, we calculated the SASA of the 11 cysteines in *ErCry4a* (Figure 4 and Table S3). Six of these residues have sidechain accessibilities greater than 20%, the other five being less than 7%. The most exposed cysteine, C317, is part of a turn near to the end of the Trp-tetrad. The next four most exposed are all located on or close to an  $\alpha$ -helix.

**Dimerization of Cysteine Mutants.** M-ZDOCK was used to identify potential dimers by docking pairs of monomers without specifying a contact residue (see below). Using a selection criterion that the sulfur atoms of the cysteines should be closer than  $\sim 6$  Å, three residues, C116, C313, and C317, were identified as possible components of intermolecular disulfides (Table S18). C116 and C317 have the highest estimated solvent exposure of all 11 cysteines, while C313 is largely buried (Figure 4 and Table S3). Four mutants of *ErCry4a* were expressed and purified with one, two, or all three of these cysteines replaced by alanines: C317A, C116A + C313A, C116A + C317A, and C116A + C313A + C317A. As judged by SDS–PAGE (Figure S1B), all four mutants oligomerize, implying that if cysteines C116, C313, and C317 are involved in dimer formation, they are not the only ones.

Two further *ErCry4a* mutants were investigated: C412A (chosen based on docking followed by MD simulations and on chemical cross-linking followed by mass spectrometric analysis, see below) and C68A + C73A + C116A + C189A + C317A (with five of the six cysteines with the largest calculated SASAs replaced by alanines). Both proteins oligomerized showing that these mutations, like the four above, might reduce the ability of *ErCry4a* to dimerize but fail to remove it completely.

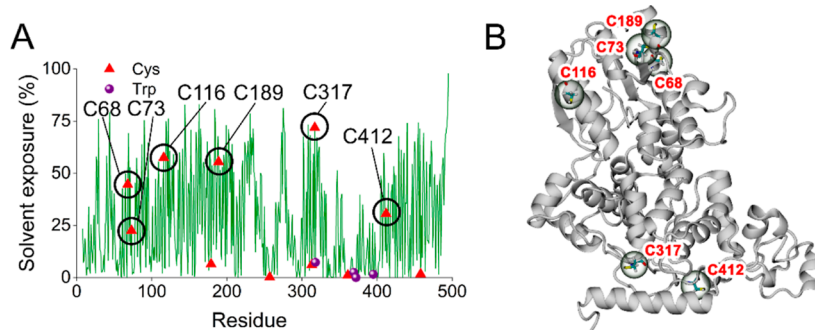


**Figure 4.** (A) Solvent exposures of residues in monomeric WT *ErCry4a* with cysteines (red triangles) indicated. Also shown (purple spheres) are the components of the Trp-tetrad: (W318, W369, W372, and W395). (B) *ErCry4a* secondary structural elements with the six most exposed cysteines indicated.

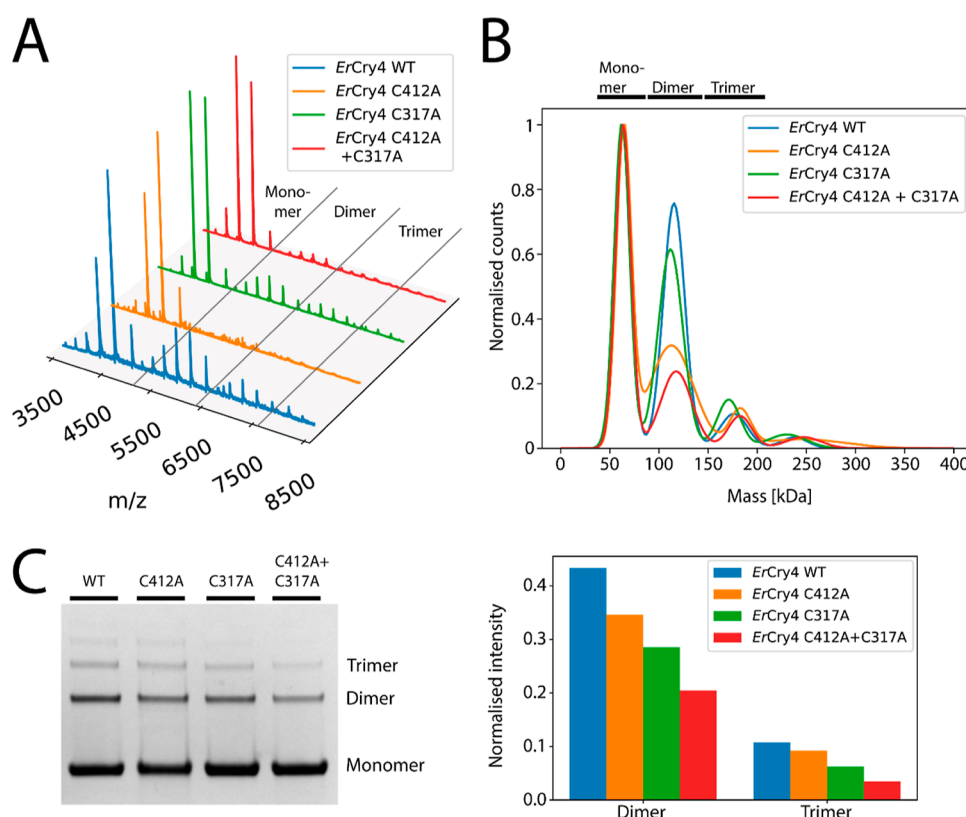


**Figure 5.** (A) Native mass spectra of WT *ErCry4a* and three cysteine mutants. All four proteins are mostly monomeric but also show charge-state envelopes from dimers and trimers. (B) MP results for the same proteins at concentrations between 13 and 15 nM displayed as Gaussian-fitted normalized counts. The four traces have been scaled so that the monomer peaks have the same height. (C) Denaturing SDS–PAGE gel for the same four proteins (full SDS–PAGE gels can be found in Figure S1C) and the normalized intensities of the protein areas.

The *ErCry4a* mutants C412A, C317A, and C412A + C317A were subsequently chosen for further comparative investigation. As seen in Figure 5, all three have a lower degree of dimerization than the WT protein, and the double mutant dimerizes less than either of the single mutants in both MP and on the gels. In the MP measurements (Figure 5B), the degree of dimer formation is in the order WT > C317A > C412A > C412A + C317A. The low concentrations used in this experiment (13–15 nM) suggest that this dimerization is largely covalent and involves both cysteines. The reversed order of C317A and C412A in Figure 5C perhaps indicates a different tendency for non-covalent and covalent association. The presence of trimers in the denaturing gel necessitates that two or more disulfide links are required for their formation.

Several of the above mutants were subsequently used to investigate the effect of blue light on dimerization. Compared to the samples kept in the dark for the same length of time, all of the proteins studied showed increased dimerization under blue light (Figure 6).

**Cysteine Accessibility Measurements.** The average number of accessible cysteines in WT and mutant forms of *ErCry4a* was determined by measuring the absorption of the product formed by treating the protein with Ellman's reagent (DTNB). The assay finds approximately five accessible cysteines for the WT protein, four for each of the C317A and C412A mutants, and three for the C116A + C317A double mutant (Table 4). More details on these absorbance measurements are given in Table S1. Assuming that each cysteine is either completely unreactive toward DTNB due to structural hindrance or reacts stoichiometrically, these results

suggest that all three of C317, C412, and C116 are significantly exposed on the surface of the protein and in principle available for the formation of intermolecular disulfide bonds. However, as a note of caution, a cysteine able to react with DTNB (a small molecule) is not necessarily accessible enough for disulfide formation between monomers.

**Cross-Linking Mass Spectrometry.** XL-MS was used to investigate the interface between monomer units in *ErCry4a* dimers by creating artificial chemical cross-links that can be cleaved by MS so as to reveal which parts of the monomers come into close contact in the dimers. The bifunctional compounds DSSO and DSBU cross-link the exposed primary amine groups of lysine residues via bis(*N*-hydroxysuccinimide) ester groups. MS analysis of peptides formed by enzymatic digestion of the cross-linked dimers identifies pairs of lysines with  $\alpha$ -carbons separated by up to  $\sim 2.7$  nm thereby constraining the location and geometry of the protein–protein interface.

Five lysines were identified to form cross-links. Based on whether they were found in the monomeric or dimeric fractions of the protein, two links were assigned to be intramolecular and three to be intermolecular, as displayed in Figure 7A. Four disulfide bonds were identified (C361–C458, C412–C361, C412–C412, and C412–C458), three of which involve C412. Of these, only C412–C412 is unequivocally intermolecular: the difficulty of distinguishing the two possibilities in a homodimer means that the other three could be intermolecular or intramolecular or both. The intermolecular K152–K152 link is consistent with a C412–C412 disulfide bond because K152 and C412 are on the same



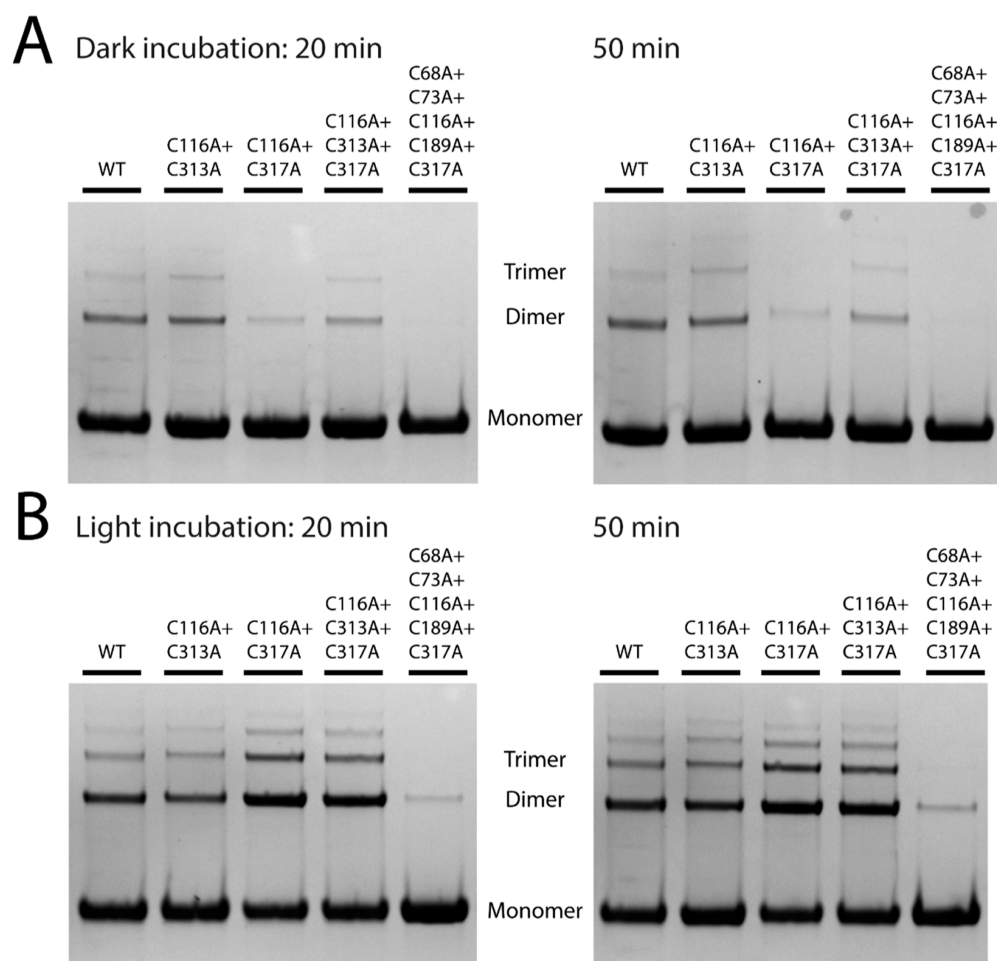


**Figure 6.** Degree of covalent dimerization as monitored by SDS–PAGE gels. The samples were incubated for 20 min under dark (A) and blue-light conditions (B) prior to running the first SDS–PAGE gel and a further 30 min before running the second one (full SDS–PAGE gels can be found in Figure S2).

**Table 4. TNB Absorbance Measurements (at 412 nm) and Average Number of Accessible Cysteines in Wild-Type and Mutant Forms of *ErCry4a***

	$A_{412}$	accessible cysteines
WT	$0.30 \pm 0.01$	$4.78 \pm 0.13$
C317A	$0.27 \pm 0.01$	$4.23 \pm 0.10$
C412A	$0.27 \pm 0.00$	$4.16 \pm 0.05$
C116A + C317A	$0.17 \pm 0.01$	$3.30 \pm 0.11$

side of the protein (Figure 7B). The links from K234 to K429 and from K152 to K507 were also found in the monomer protein fraction suggesting that they are more likely to be intramonomer. For more details see Table S2. Overall, these results point to C412 as a likely component of disulfide links between monomers.

**Computationally Reconstructed *ErCry4a* Dimer Structures.** As described in the Methods Section (Figure 2), a large number of covalently and non-covalently bound dimers were constructed using ZDOCK and M-ZDOCK. A total of 49 docked structures were generated for a truncated form of *ErCry4a* (Table 3) using the seven most exposed cysteines as contact residues. Another ten were obtained without specifying which cysteines should be near one another in the docked structure. Twelve of these structures were selected for MD simulations, based on the separations of the

cysteine residues (eight with a C412–C412 disulfide, three with C317–C317, and one with C189–C485). To these were added: a non-covalently bound structure derived from the crystallographic dimer of mouse Cry2, a dimer with two disulfide bridges, and two structures for the FL form of *ErCry4a*, both non-covalent.

Of the 16 dimer structures chosen for MD simulation (see Methods Section and Supporting Information for more details), seven were selected (Table 5) on the basis of their monomer–monomer interaction energies,  $E_{\text{tot}}$ : two structures with C412–C412 disulfides ( $\text{cov}^{412A}$  and  $\text{cov}^{412B}$ ), two with C317–C317 bonds ( $\text{cov}^{317A}$  and  $\text{cov}^{317B}$ ), two non-covalent ( $\text{ncov}^A$  and  $\text{ncov}^M$ ), and the one with two disulfides ( $\text{cov}^D$ , C116–C313 and C313–C116).  $\text{ncov}^M$  is the structure based on the crystallographic dimer of *MmCry2*.

Various other properties of these structures, derived from the MD simulations, are presented in Table 5 and described below. Of the seven dimers,  $\text{ncov}^A$  and  $\text{cov}^{412A}$  have the largest internal potential energies ( $-E_{\text{tot}}$ ) and are therefore the most stable. The interaction between the monomers in  $\text{ncov}^A$  is probably stronger because the disulfide bond in  $\text{cov}^{412A}$  (and the other covalent structures) constrains the monomers at the dimer interface preventing them finding more favorable binding conformations. Note that  $E_{\text{tot}}$  comprises the non-covalent van der Waals and electrostatic interactions between the monomers and does not include the ca. 60 kcal mol<sup>−1</sup>

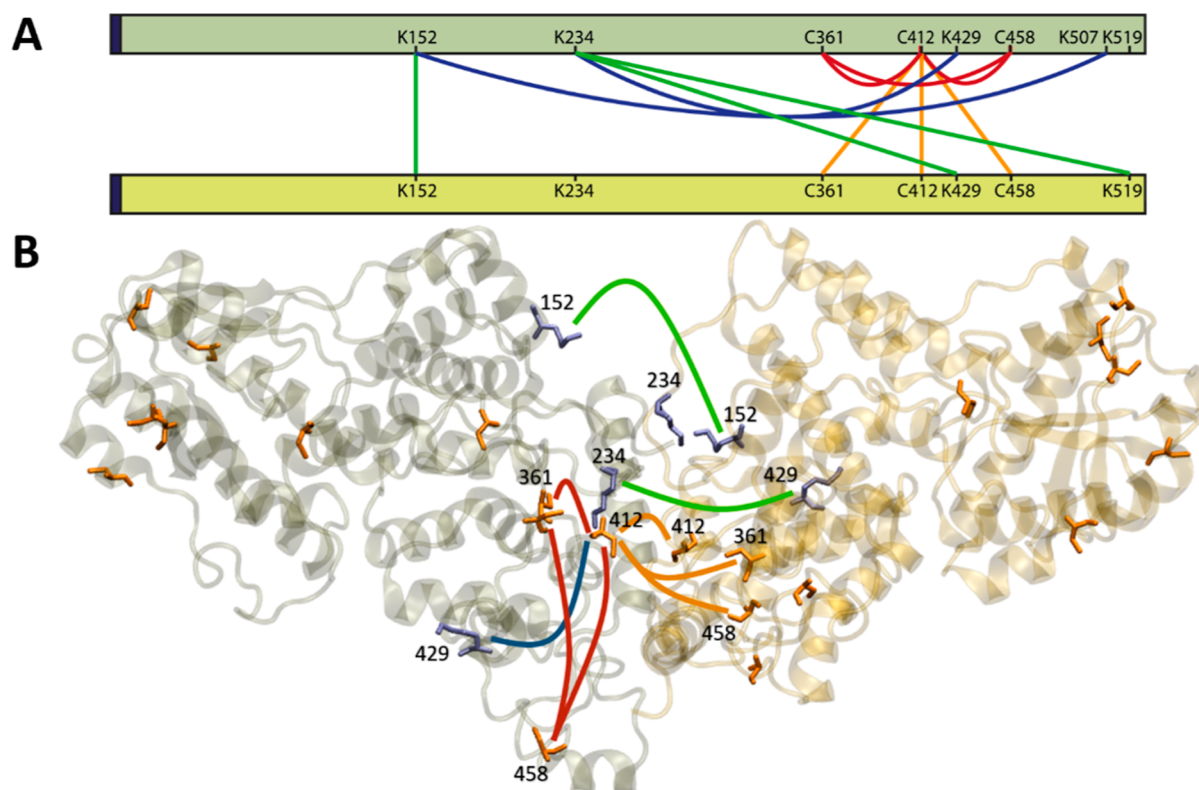


**Figure 7.** (A) Network plot of cross-linking sites found for *ErCry4a*. The orange and red lines are potential inter- and intramonomer disulfide bonds, respectively. The inter- and intramonomer cross-links formed by DSSU and DSSO are shown in green and blue, respectively. The dark blue region at the N-terminus (left hand side) corresponds to the five additional amino acids that remained after His-tag cleavage. (B) Graphical representation of a possible coordination of two *ErCry4a* monomers. The cross-links are drawn with the same color code as in (A). Cysteine residues are shown in orange and lysine residues in purple. Only residues 1–495 are displayed.

**Table 5. Seven Simulated and Analyzed *ErCry4a* Dimers with the Largest Non-Bonded Monomer–Monomer Interaction Energies,  $E_{\text{tot}}$ <sup>a</sup>**

dimer	$-E_{\text{tot}}/\text{kcal mol}^{-1}$	$R_g/\text{\AA}$	RMSD/ $\text{\AA}$	RMSF/ $\text{\AA}$	$A_{\text{IS}}/\text{\AA}^2$	hydrogen bonds	salt bridges
ncov <sup>A</sup>	857 ± 85	35.2 ± 0.3	3.5 ± 0.4	2.2 ± 1.0	2762 ± 292	106	29
cov <sup>412A</sup>	526 ± 83	41.2 ± 0.2	2.5 ± 0.4	5.7 ± 1.3	1840 ± 115	31	13
ncov <sup>M</sup>	505 ± 163	33.0 ± 0.3	3.4 ± 1.4	2.3 ± 1.0	2442 ± 284	111	12
cov <sup>412B</sup>	437 ± 127	41.4 ± 0.7	6.2 ± 2.8	5.4 ± 1.5	1040 ± 310	49	12
cov <sup>317A</sup>	186 ± 103	38.3 ± 0.3	4.0 ± 0.6	1.8 ± 0.9	1082 ± 220	64	10
cov <sup>D</sup>	178 ± 44	33.0 ± 0.2	2.5 ± 0.3	1.3 ± 0.7	2140 ± 330	47	3
cov <sup>317B</sup>	171 ± 73	38.5 ± 0.2	3.8 ± 0.8	1.8 ± 0.9	1070 ± 110	59	12

<sup>a</sup>Results for other dimers are given in the [Supporting Information](#). The various parameters are discussed in the text.

expected for a disulfide bond.<sup>80</sup> The other dimers featured in [Table 5](#), especially cov<sup>317A</sup>, cov<sup>D</sup>, and cov<sup>317B</sup>, have smaller interaction energies and are therefore less likely to be formed.

The stronger binding of the two non-covalent dimers is reflected in their smaller radius of gyration,  $R_g$ , which is a measure of the compactness of the structure. The cov<sup>D</sup> dimer also has a relatively small  $R_g$  presumably because of the constraining effects of its two disulfide bonds.

Another indication of protein stability is provided by the average root-mean-square deviation (RMSD) of the backbone atom positions from those in a reference structure immediately prior to the production simulation.<sup>81</sup> Smaller values of this parameter correspond to dimers in which the initial docked structure did not alter significantly throughout the simulation. Apart from cov<sup>412B</sup> (6.2  $\text{\AA}$ ), all the dimers in [Table 5](#) have RMSDs less than 4  $\text{\AA}$ . Dimers cov<sup>412A</sup> and cov<sup>D</sup> (RMSD  $\approx$  2.5  $\text{\AA}$ ) are the most stable as judged by this measure.

A parameter that quantifies the degree of internal mobility of the dimer is the root-mean-square amplitude of the structural fluctuations (RMSFs) during the course of an MD simulation. RMSF values were calculated by comparing the positions of each carbon atom at every simulation step to its position in the average structure. With the exception of cov<sup>317B</sup>, which is much less rigid than the others, all the structures in [Table 5](#) have comparable values of this parameter. Certain regions of the monomers are more flexible than others, in particular the C-terminal extension (residues 470–495) and the phosphate-binding loop (residues 231–248). For the most part, this flexibility seems to be retained on dimerization.

A further measure of the interaction between the monomer units of a dimer is the interaction surface area,  $A_{\text{IS}}$  ([Table 5](#)), defined as the difference between the solvent accessible surface areas of the separate monomers and that of the dimer. Larger values of  $A_{\text{IS}}$  should correlate with stronger binding energies

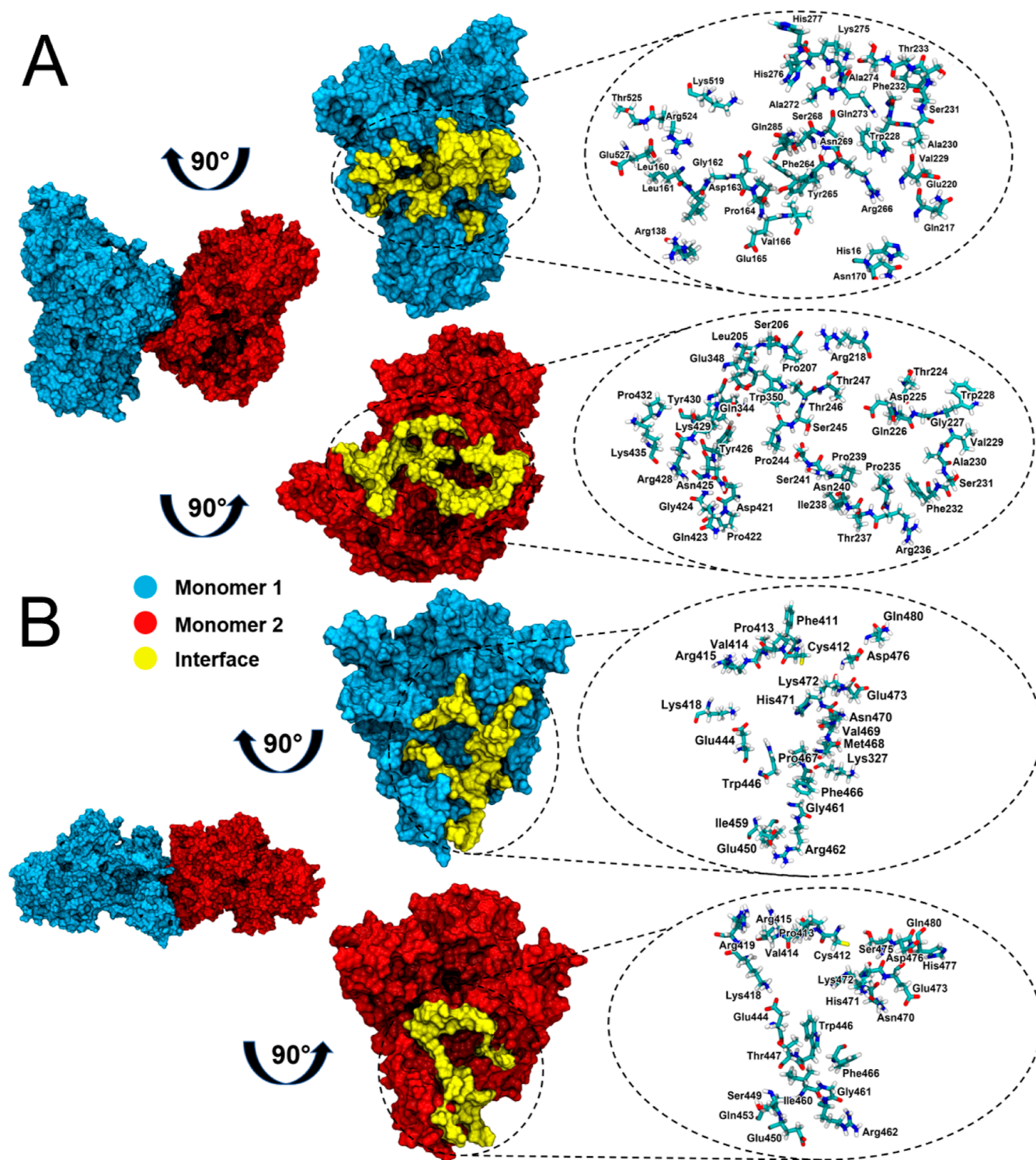


**Figure 8.** The dimer interfaces of (A)  $ncov^A$  and (B)  $cov^{412A}$ . Left: dimer structures. Middle: 90°-rotated monomers showing the interacting residues (yellow). Right: representations of the contact residues in the interface.

( $-E_{tot}$ ), as seems to be broadly the case for the dimers in Table 5. Two additional parameters are the number of hydrogen bonds and the number of salt bridges that link the two components of the dimer. Only salt bridges present in more than 10% of the MD frames were counted. All values have been averaged over the duration of the corresponding MD simulations. The two non-covalent structures have the largest

interaction surface areas and many more hydrogen bonds than the covalently bound dimers.

Figure 8A,B shows the dimer interfaces of  $cov^{412A}$  and  $ncov^A$ . Consistent with the data in Table 5, the non-covalent dimer has a more extensive interface.

As described in the Methods Section, none of the docked dimers obtained using C68, C73, C116, and C179 as the contact residue were deemed worth simulating by MD. These



four residues, together with the four with the smallest solvent accessibilities (C257, C313, C361, and C458) appear to have a low propensity to dimerize via the formation of a single disulfide bond. All of the C189-linked dimers which satisfied our conditions for MD simulation had smaller binding energies than the seven in Table S and therefore appear less likely to be formed. Of the covalently bound dimers, this leaves C317–C317, C412–C412, and the double-disulfide dimer, cov<sup>D</sup>, which involves C116 and C313. Based on the data in Table S, C412 seems most likely to form covalent links between *ErCry4a* monomers. As more than one cysteine could be involved in covalent dimer formation, the cov<sup>412A</sup> dimer was further checked for the possibility of an additional disulfide bond, but none could be identified (Figure S16). Additionally, the formation of the dimers most likely does not involve the CTTs, as shown in Table S20 in the Supporting Information. The other main conclusion that can be drawn from these studies is that the possibility of non-covalently bound dimers cannot be dismissed.

## CONCLUSIONS

The experiments described here show that *ErCry4a* readily forms dimers and that they are covalently linked by disulfide bonds. This process is promoted by exposure to blue light. Several cysteines seem to be involved, C317 and C412 being the most likely. Computational modeling supports this conclusion, provides insights into the relative orientation of the monomer units, and suggests that non-covalently bound dimers may also be relatively stable. The relevance of these findings to the proposed role of *Cry4a* in avian magnetoreception is unclear.

That *ErCry4a* dimers are not readily disrupted in a reducing environment (10 mM DTT, Figure 3) suggest that they could persist in vivo. Despite the reducing environment of the cell, there are well-documented examples of biologically significant intra-cellular disulfide-linked proteins involved in redox processes.<sup>82–84</sup> Moreover, little is known about the redox conditions in the avian photoreceptor cells that are thought to contain the magnetoreceptors. It therefore seems premature to exclude the possibility that *ErCry4a* dimerization could have a biological function.

If *ErCry4a* does have a role in magnetic sensing and/or signaling, then an immediate question is why the protein has evolved to stabilize inter-monomer disulfide bonds to the extent that only a proportion of the proteins dimerize under the conditions of the experiments reported here. One explanation is that these dimers are simply aggregates of unfolded monomers. However, we think this is unlikely, as the *ErCry4a* dimers bind FAD and have native MS charge-state distributions that are similar to those of the monomers suggesting that the protein remains correctly folded and therefore potentially functional in the dimeric state. Partially unfolded proteins typically display higher charge states than the native states. An alternative explanation is that a monomer–dimer equilibrium could play a regulatory role in magnetic sensing or signal transduction. This would also be supported by the finding that dimerization is promoted by blue light which could conceivably be the first step of a signaling cascade. Activation of plant *Cry*s 1 and 2 leads to homo-oligomerization.<sup>3,5,40,41,85</sup> Additionally, the formation of a disulfide bond influences the interaction between mouse *Cry* 1 and the circadian protein period (PER) and depends on the metabolic/oxidative state inside the cell.<sup>86</sup> Taken together,

these examples show that photoactivation of some *Cry*s causes oligomerization and that *Cry*'s affinity for other proteins could rely on disulfide bond formation.

An observation reported by Xu et al.<sup>15</sup> (in Figure S5) may be relevant here. The samples of *ErCry4a* that had been purified without adding 10 mM BME to prevent dimerization showed clear evidence for the formation of relatively long-lived (nanosecond to microsecond) photo-excited singlet (<sup>S</sup>FAD\*) and triplet (<sup>T</sup>FAD\*) states of FAD in addition to the normal photo-induced electron transfer reactions that generate radical pairs. It was speculated that subtle differences in protein conformation, induced by dimerization, might inhibit electron transfer from the tryptophan tetrad to <sup>S</sup>FAD\*, thereby stabilizing <sup>S</sup>FAD\* and allowing formation of <sup>T</sup>FAD\* by intersystem crossing. The samples of *ErCry4a* purified with 10 mM BME, and therefore more likely to be monomeric, showed much weaker signals from <sup>S</sup>FAD\* and <sup>T</sup>FAD\*.

While recognizing that the experiments described here have not been performed in cells, they do show it is quite possible that dimerization could have an impact on the in vivo function of avian *Cry*s and provide an incentive for further work in this area.

## ASSOCIATED CONTENT

### Supporting Information

The Supporting Information is available free of charge at <https://pubs.acs.org/doi/10.1021/acs.jpcb.3c01305>.

Full SDS–PAGE gels, peak isolation using native MS and XL-MS, photometric cysteine-exposure measurements, solvent exposure calculations, ranking of dimeric structures within a dimer family, detailed cysteine distance-analysis of docked structures, the molecular dynamics protocol, and an analysis of the involvement of C-terminal tails in dimer formation (PDF)

## AUTHOR INFORMATION

### Corresponding Author

**Iliia A. Solovyov** – Institute of Physics, Carl von Ossietzky University of Oldenburg, Oldenburg 26129, Germany; Research Center for Neurosensory Sciences, Carl von Ossietzky University of Oldenburg, Oldenburg 26111, Germany; Center for Nanoscale Dynamics (CENAD), Carl von Ossietzky Universität Oldenburg, Oldenburg 26129, Germany; [orcid.org/0000-0002-8626-145X](https://orcid.org/0000-0002-8626-145X); Email: [ilia.solovyov@uni-oldenburg.de](mailto:ilia.solovyov@uni-oldenburg.de)

### Authors

**Maja Hanić** – Institute of Physics, Carl von Ossietzky University of Oldenburg, Oldenburg 26129, Germany

**Lewis M. Antill** – Graduate School of Science and Engineering, Saitama University, Saitama 338-8570, Japan; Japan Science and Technology Agency, Precursory Research for Embryonic Science and Technology, Kawaguchi, Saitama 332-0012, Japan

**Angela S. Gehrckens** – Department of Chemistry, Physical & Theoretical Chemistry Laboratory, University of Oxford, Oxford OX1 3QZ, U.K.

**Jessica Schmidt** – Department of Biology and Environmental Sciences, Carl von Ossietzky University of Oldenburg, Oldenburg 26129, Germany

- Katharina Görtemaker** – Department of Neuroscience, Division of Biochemistry, Carl von Ossietzky University of Oldenburg, Oldenburg D-26111, Germany
- Rabea Bartölke** – Department of Biology and Environmental Sciences, Carl von Ossietzky University of Oldenburg, Oldenburg 26129, Germany
- Tarick J. El-Baba** – Department of Chemistry, Physical & Theoretical Chemistry Laboratory, University of Oxford, Oxford OX1 3QZ, U.K.; Kavli Institute for NanoScience Discovery, University of Oxford, Oxford OX1 3QU, U.K.; [orcid.org/0000-0003-4497-9938](https://orcid.org/0000-0003-4497-9938)
- Jingjing Xu** – Department of Biology and Environmental Sciences, Carl von Ossietzky University of Oldenburg, Oldenburg 26129, Germany
- Karl-Wilhelm Koch** – Department of Neuroscience, Division of Biochemistry, Carl von Ossietzky University of Oldenburg, Oldenburg D-26111, Germany; Research Center for Neurosensory Sciences, Carl von Ossietzky University of Oldenburg, Oldenburg 26111, Germany; [orcid.org/0000-0003-1501-0044](https://orcid.org/0000-0003-1501-0044)
- Henrik Mouritsen** – Department of Biology and Environmental Sciences, Carl von Ossietzky University of Oldenburg, Oldenburg 26129, Germany; Research Center for Neurosensory Sciences, Carl von Ossietzky University of Oldenburg, Oldenburg 26111, Germany
- Justin L. P. Benesch** – Department of Chemistry, Physical & Theoretical Chemistry Laboratory, University of Oxford, Oxford OX1 3QZ, U.K.; Kavli Institute for NanoScience Discovery, University of Oxford, Oxford OX1 3QU, U.K.; [orcid.org/0000-0002-1507-3742](https://orcid.org/0000-0002-1507-3742)
- P. J. Hore** – Department of Chemistry, Physical & Theoretical Chemistry Laboratory, University of Oxford, Oxford OX1 3QZ, U.K.; [orcid.org/0000-0002-8863-570X](https://orcid.org/0000-0002-8863-570X)

Complete contact information is available at:  
<https://pubs.acs.org/10.1021/acs.jpcb.3c01305>

## Author Contributions

♦M.H., L.M.A., and A.S.G. are contributed equally.

## Notes

The authors declare no competing financial interest.

## ACKNOWLEDGMENTS

The authors would like to thank the Volkswagen Foundation (Lichtenberg Professorship to I.A.S.), the Deutsche Forschungsgemeinschaft (DFG; GRK1885: Molecular Basis of Sensory Biology and SFB 1372: Magnetoreception and Navigation in Vertebrates), the Ministry for Science and Culture of Lower Saxony [Simulations Meet Experiments on the Nanoscale: Opening up the Quantum World to Artificial Intelligence (SMART) and Dynamik auf der Nanoskala: Von kohärenten Elementarprozessen zur Funktionalität (DyNano)], the Japan Science and Technology Agency (JST) PRESTO (Quantum Bio) grant no. JPMJPR19G1 (L.M.A.), the European Research Council (under the European Union's Horizon 2020 research and innovation program, grant agreement no. 810002, Synergy Grant: *QuantumBirds*), and the Office of Naval Research Global, award no. N62909-19-1-2045. Computational resources for the simulations were provided by the CARL Cluster at the Carl-von-Ossietzky University, Oldenburg, supported by the DFG and the Ministry for Science and Culture of Lower Saxony. The authors gratefully acknowledge the computing time granted by

the Resource Allocation Board and provided on the super-computer Lise and Emmy at NHR@ZIB and NHR@Göttingen as part of the NHR infrastructure. The calculations for this research were conducted with computing resources under the project nip00058. T.J.E. was supported by funds from the Royal Society under a Royal Society Newton International Fellowship. A.S.G. is grateful to Mark Pepys who provided CRP for the mass spectrometric investigation and to Josh Bishop who helped with the mass photometry measurements and data analysis.

## REFERENCES

- (1) Matthews, J. M. *Protein Dimerization and Oligomerization in Biology*; Springer Science + Business Media, LLC: Sydney, Australia, 2012.
- (2) Heldin, C.-H. Dimerization of Cell Surface Receptors in Signal Transduction. *Cell* **1995**, *80*, 213–223.
- (3) Palayam, M.; Ganapathy, J.; Guercio, A. M.; Tal, L.; Deck, S. L.; Shabek, N. Structural Insights into Photoactivation of Plant Cryptochrome-2. *Commun. Biol.* **2021**, *4*, 28.
- (4) Poehn, B.; Krishnan, S.; Zurl, M.; Coric, A.; Rokvic, D.; Orel, L.; Raible, F.; Wolf, E.; Tessmar-Raible, K. A Cryptochrome Adopts Distinct Moon- and Sunlight States and Functions as Moonlight Interpreter in Monthly Oscillator Entrainment. *Nat. Commun.* **2022**, *13*, 5220.
- (5) Shao, K.; Zhang, X.; Li, X.; Hao, Y.; Huang, X.; Ma, M.; Zhang, M.; Yu, F.; Liu, H.; Zhang, P. The Oligomeric Structures of Plant Cryptochromes. *Nat. Struct. Mol. Biol.* **2020**, *27*, 480–488.
- (6) Yu, X.; Liu, H.; Klejnot, J.; Lin, C. The Cryptochrome Blue Light Receptors. *The Arabidopsis book*; American Society of Plant Biologists, 2010; Vol. 2010, p 01355.
- (7) Chaves, I.; Pokorny, R.; Byrdin, M.; Hoang, N.; Ritz, T.; Brettel, K.; Essen, L. O.; Van Der Horst, G. T. J.; Batschauer, A.; Ahmad, M. The Cryptochromes: Blue Light Photoreceptors in Plants and Animals. *Annu. Rev. Plant Biol.* **2011**, *62*, 335–364.
- (8) Brudler, R.; Hitomi, K.; Daiyasu, H.; Toh, H.; Kucho, K. I.; Ishiura, M.; Kanehisa, M.; Roberts, V. A.; Todo, T.; Tainer, J. A.; Getzoff, E. D. Identification of a New Cryptochrome Class: Structure, Function, and Evolution. *Mol. Cell* **2003**, *11*, 59–67.
- (9) Navarro, E.; Niemann, N.; Kock, D.; Dadaeva, T.; Gutiérrez, G.; Engelsdorf, T.; Kiontke, S.; Corrochano, L. M.; Batschauer, A.; Garre, V. The DASH-Type Cryptochrome from the Fungus *Mucor Circinelloides* Is a Canonical CPD-Photolyase. *Curr. Biol.* **2020**, *30*, 4483–4490.
- (10) Michael, A. K.; Fribourgh, J. L.; Van Gelder, R. N.; Partch, C. L. Animal Cryptochromes: Divergent Roles in Light Perception, Circadian Timekeeping and Beyond. *Photochem. Photobiol.* **2017**, *93*, 128–140.
- (11) Cashmore, A. R.; Jarillo, J. A.; Wu, Y. J.; Liu, D. Cryptochromes: Blue Light Receptors for Plants and Animals. *Science* **1999**, *284*, 760–765.
- (12) Ozturk, N. Phylogenetic and Functional Classification of the Photolyase/Cryptochrome Family. *Photochem. Photobiol.* **2017**, *93*, 104–111.
- (13) Malhotra, K.; Kim, S. T.; Batschauer, A.; Dawut, L.; Sancar, A. Putative Blue-Light Photoreceptors from *Arabidopsis thaliana* and *Sinapis alba* with a High Degree of Sequence Homology to DNA Photolyase Contain the Two Photolyase Cofactors but Lack DNA Repair Activity. *Biochemistry* **1995**, *34*, 6892–6899.
- (14) Parico, G. C. G.; Partch, C. L. The Tail of Cryptochromes: An Intrinsically Disordered Cog within the Mammalian Circadian Clock. *Cell Commun. Signaling* **2020**, *18*, 182.
- (15) Xu, J.; Jarocha, L. E.; Zollitsch, T.; Konowalczyk, M.; Henbest, K. B.; Richert, S.; Golesworthy, M. J.; Schmidt, J.; Déjean, V.; Sowood, D. J. C.; et al. Magnetic Sensitivity of Cryptochrome 4 from a Migratory Songbird. *Nature* **2021**, *594*, 535–540.
- (16) Ritz, T.; Adem, S.; Schulten, K. A Model for Photoreceptor-Based Magnetoreception in Birds. *Biophys. J.* **2000**, *78*, 707–718.

- (17) Solov'yov, I. A.; Domratcheva, T.; Moughal Shahi, A. R.; Schulten, K. Decrypting Cryptochrome: Revealing the Molecular Identity of the Photoactivation Reaction. *J. Am. Chem. Soc.* **2012**, *134*, 18046–18052.
- (18) Hore, P. J.; Mouritsen, H. The Radical-Pair Mechanism of Magnetoreception. *Annu. Rev. Biophys.* **2016**, *45*, 299–344.
- (19) Wong, S. Y.; Solov'yov, I. A.; Hore, P. J.; Kattinig, D. R. Nuclear Polarization Effects in Cryptochrome-Based Magnetoreception. *J. Chem. Phys.* **2021**, *154*, 035102.
- (20) Maeda, K.; Robinson, A. J.; Henbest, K. B.; Hogben, H. J.; Biskup, T.; Ahmad, M.; Schleicher, E.; Weber, S.; Timmel, C. R.; Hore, P. J. Magnetically Sensitive Light-Induced Reactions in Cryptochrome Are Consistent with Its Proposed Role as a Magnetoreceptor. *Proc. Natl. Acad. Sci.* **2012**, *109*, 4774–4779.
- (21) Mouritsen, H.; Janssen-Bienhold, U.; Liedvogel, M.; Feenders, G.; Stalleicken, J.; Dirks, P.; Weiler, R. Cryptochromes and Neuronal-Activity Markers Colocalize in the Retina of Migratory Birds during Magnetic Orientation. *Proc. Natl. Acad. Sci. U.S.A.* **2004**, *101*, 14294–14299.
- (22) Möller, A.; Sagasser, S.; Wiltshko, W.; Schierwater, B. Retinal Cryptochrome in a Migratory Passerine Bird: A Possible Transducer for the Avian Magnetic Compass. *Naturwissenschaften* **2004**, *91*, 585–588.
- (23) Nießner, C.; Denzau, S.; Gross, J. C.; Peichl, L.; Bischof, H. J.; Fleissner, G.; Wiltshko, W.; Wiltshko, R. Avian Ultraviolet/Violet Cones Identified as Probable Magnetoreceptors. *PLoS One* **2011**, *6*, No. e20091.
- (24) Nießner, C.; Gross, J. C.; Denzau, S.; Peichl, L.; Fleissner, G.; Wiltshko, W.; Wiltshko, R. Seasonally Changing Cryptochrome 1b Expression in the Retinal Ganglion Cells of a Migrating Passerine Bird. *PLoS One* **2016**, *11*, No. e0150377.
- (25) Bolte, P.; Bleibaum, F.; Einwich, A.; Günther, A.; Liedvogel, M.; Heyers, D.; Depping, A.; Wöhlbrand, L.; Rabus, R.; Janssen-bienhold, U.; et al. Localisation of the Putative Magnetoreceptive Protein Cryptochrome 1b in the Retinae of Migratory Birds and Homing Pigeons. *PLoS One* **2016**, *11*, 0147819.
- (26) Bolte, P.; Einwich, A.; Seth, P. K.; Chetverikova, R.; Heyers, D.; Wojahn, I.; Janssen-Bienhold, U.; Feederle, R.; Hore, P.; Dedek, K.; et al. Cryptochrome 1a Localisation in Light- and Dark-Adapted Retinae of Several Migratory and Non-Migratory Bird Species: No Signs of Light-Dependent Activation. *Ethol. Ecol. Evol.* **2021**, *33*, 248–272.
- (27) Einwich, A.; Seth, P. K.; Bartölke, R.; Bolte, P.; Feederle, R.; Dedek, K.; Mouritsen, H. Localisation of Cryptochrome 2 in the Avian Retina. *J. Comp. Physiol., A* **2022**, *208*, 69–81.
- (28) Zoltowski, B. D.; Chelliah, Y.; Wickramaratne, A.; Jarocho, L.; Karki, N.; Xu, W.; Mouritsen, H.; Hore, P. J.; Hibbs, R. E.; Green, C. B.; et al. Chemical and Structural Analysis of a Photoactive Vertebrate Cryptochrome from Pigeon. *Proc. Natl. Acad. Sci. U.S.A.* **2019**, *116*, 19449–19457.
- (29) Günther, A.; Einwich, A.; Sjulstok, E.; Feederle, R.; Bolte, P.; Koch, K.-W. W.; Solov'yov, I. A.; Mouritsen, H. Double-Cone Localization and Seasonal Expression Pattern Suggest a Role in Magnetoreception for European Robin Cryptochrome 4. *Curr. Biol.* **2018**, *28*, 211–223.e4.
- (30) Ozturk, N.; Selby, C. P.; Song, S. H.; Ye, R.; Tan, C.; Kao, Y. T.; Zhong, D.; Sancar, A. Comparative Photochemistry of Animal Type 1 and Type 4 Cryptochromes. *Biochemistry* **2009**, *48*, 8585–8593.
- (31) Hochstoeger, T.; Al Said, T.; Maestre, D.; Walter, F.; Vilceanu, A.; Pedron, M.; Cushion, T. D.; Snider, W.; Nimpf, S.; Nordmann, G. C.; et al. The Biophysical, Molecular, and Anatomical Landscape of Pigeon CRY4: A Candidate Light-Based Quantal Magnetosensor. *Sci. Adv.* **2020**, *6*, No. eabb9110.
- (32) Chetverikova, R.; Dautaj, G.; Schwigon, L.; Dedek, K.; Mouritsen, H. Double Cones in the Avian Retina Form an Oriented Mosaic Which Might Facilitate Magnetoreception and/or Polarized Light Sensing. *J. R. Soc., Interface* **2022**, *19*, 20210877.
- (33) Balay, S. D.; Hochstoeger, T.; Vilceanu, A.; Malkemper, E. P.; Snider, W.; Dürnberger, G.; Mechtler, K.; Schuechner, S.; Ogris, E.; Nordmann, G. C.; et al. The Expression, Localisation and Interactome of Pigeon CRY2. *Sci. Rep.* **2021**, *11*, 20293.
- (34) Einwich, A.; Dedek, K.; Seth, P. K.; Laubinger, S.; Mouritsen, H. A Novel Isoform of Cryptochrome 4 (Cry4b) Is Expressed in the Retina of a Night-Migratory Songbird. *Sci. Rep.* **2020**, *10*, 15794.
- (35) Kattinig, D. R.; Nielsen, C.; Solov'yov, I. A. Molecular Dynamics Simulations Disclose Early Stages of the Photo-Activation of Cryptochrome 4. *New J. Phys.* **2018**, *20*, 083018.
- (36) Schuhmann, F.; Kattinig, D. R.; Solov'yov, I. A. Exploring Post-Activation Conformational Changes in Pigeon Cryptochrome 4. *J. Phys. Chem. B* **2021**, *125*, 9652–9659.
- (37) Chandrasekaran, S.; Schneps, C. M.; Dunleavy, R.; Lin, C.; DeOliveira, C. C.; Ganguly, A.; Crane, B. R. Tuning Flavin Environment to Detect and Control Light-Induced Conformational Switching in *Drosophila* Cryptochrome. *Commun. Biol.* **2021**, *4*, 249.
- (38) Watari, R.; Yamaguchi, C.; Zemba, W.; Kubo, Y.; Okano, K.; Okano, T. Light-Dependent Structural Change of Chicken Retinal Cryptochrome 4. *J. Biol. Chem.* **2012**, *287*, 42634–42641.
- (39) Kondoh, M.; Shiraishi, C.; Müller, P.; Ahmad, M.; Hitomi, K.; Getzoff, E. D.; Terazima, M. Light-Induced Conformational Changes in Full-Length *Arabidopsis thaliana* Cryptochrome. *J. Mol. Biol.* **2011**, *413*, 128–137.
- (40) Rosenfeldt, G.; Viana, R. M.; Mootz, H. D.; Von Arnim, A. G.; Batschauer, A. Chemically Induced and Light-Independent Cryptochrome Photoreceptor Activation. *Mol. Plant* **2008**, *1*, 4–14.
- (41) Sang, Y.; Li, Q. H.; Rubio, V.; Zhang, Y. C.; Mao, J.; Deng, X. W.; Yang, H. Q. N-Terminal Domain-Mediated Homodimerization Is Required for Photoreceptor Activity of *Arabidopsis* Cryptochrome 1. *Plant Cell* **2005**, *17*, 1569–1584.
- (42) Park, H.; Kim, N. Y.; Lee, S.; Kim, N.; Kim, J.; Heo, W. Do. Optogenetic Protein Clustering through Fluorescent Protein Tagging and Extension of CRY2. *Nat. Commun.* **2017**, *8*, 30.
- (43) Wu, H.; Scholten, A.; Einwich, A.; Mouritsen, H.; Koch, K. W. Protein-Protein Interaction of the Putative Magnetoreceptor Cryptochrome 4 Expressed in the Avian Retina. *Sci. Rep.* **2020**, *10*, 7364.
- (44) Görtemaker, K.; Yee, C.; Bartölke, R.; Behrmann, H.; Voß, J. O.; Schmidt, J.; Xu, J.; Solovyeva, V.; Leberecht, B.; Behrmann, E.; et al. Direct Interaction of Avian Cryptochrome 4 with a Cone Specific G-Protein. *Cells* **2022**, *11*, 2043.
- (45) Levy, C.; Zoltowski, B. D.; Jones, A. R.; Vaidya, A. T.; Top, D.; Widom, J.; Young, M. W.; Scrutton, N. S.; Crane, B. R.; Leys, D. Updated Structure of *Drosophila* Cryptochrome. *Nature* **2013**, *495*, E3–E4.
- (46) Miller, S.; Son, Y. L.; Aikawa, Y.; Makino, E.; Nagai, Y.; Srivastava, A.; Oshima, T.; Sugiyama, A.; Hara, A.; Abe, K.; et al. Isoform-Selective Regulation of Mammalian Cryptochromes. *Nat. Chem. Biol.* **2020**, *16*, 676–685.
- (47) Czarna, A.; Berndt, A.; Singh, H. R.; Grudziecki, A.; Ladurner, A. G.; Timinszky, G.; Kramer, A.; Wolf, E. Structures of *Drosophila* Cryptochrome and Mouse Cryptochrome1 Provide Insight into Circadian Function. *Cell* **2013**, *153*, 1394–1405.
- (48) Kondrat, D. L. F.; Struwe, W. B.; Benesch, J. L. P. Structural Proteomics: High-Throughput Methods: Second Edition. In *Structural Proteomics: High-Throughput Methods*, 2nd ed.; Owens, R. J., Ed.; Springer Science & Business Media: New York, 2015; Vol. 1261, pp 1–371.
- (49) Lazar, I. J.; Lazar, I. S. *GelAnalyzer 19.1*, 2022. [www.gelanalyzer.com](http://www.gelanalyzer.com) (accessed Mar 23, 2022).
- (50) Young, G.; Hundt, N.; Cole, D.; Fineberg, A.; Andrecka, J.; Tyler, A.; Olerinyova, A.; Ansari, A.; Marklund, E. G.; Collier, M. P.; et al. Quantitative mass imaging of single biological macromolecules. *Science* **2018**, *360*, 423–427.
- (51) Kao, A.; Chiu, C.; Vellucci, D.; Yang, Y.; Patel, V. R.; Guan, S.; Randall, A.; Baldi, P.; Rychnovsky, S. D.; Huang, L. Development of a Novel Cross-Linking Strategy for Fast and Accurate Identification of



Cross-Linked Peptides of Protein Complexes. *Mol. Cell. Proteomics* **2011**, *10*, M110.002170.

(52) Müller, M. Q.; Dreier, F.; Ihling, C. H.; Schäfer, M.; Sinz, A. Cleavable Cross-Linker for Protein Structure Analysis: Reliable Identification of Cross-Linking Products by Tandem MS. *Anal. Chem.* **2010**, *82*, 6958–6968.

(53) Iacobucci, C.; Götz, M.; Ihling, C. H.; Piotrowski, C.; Arlt, C.; Schäfer, M.; Hage, C.; Schmidt, R.; Sinz, A. A Cross-Linking/Mass Spectrometry Workflow Based on MS-Cleavable Cross-Linkers and the MeroX Software for Studying Protein Structures and Protein–Protein Interactions. *Nat. Protoc.* **2018**, *13*, 2864–2889.

(54) Shevchenko, A.; Tomas, H.; Havli, J.; Olsen, J. V.; Mann, M. In-Gel Digestion for Mass Spectrometric Characterization of Proteins and Proteomes. *Nat. Protoc.* **2007**, *1*, 2856–2860.

(55) Götz, M.; Pettelkau, J.; Fritzsche, R.; Ihling, C. H.; Schäfer, M.; Sinz, A. Automated Assignment of MS/MS Cleavable Cross-Links in Protein 3D-Structure Analysis. *J. Am. Soc. Mass Spectrom.* **2014**, *26*, 83–97.

(56) Helten, A.; Koch, K. W. Calcium-Dependent Conformational Changes in Guanylate Cyclase-Activating Protein 2 Monitored by Cysteine Accessibility. *Biochem. Biophys. Res. Commun.* **2007**, *356*, 687–692.

(57) Fraczek, R.; Braun, W. Exact and Efficient Analytical Calculation of the Accessible Surface Areas and Their Gradients for Macromolecules. *J. Comput. Chem.* **1998**, *19*, 319–333.

(58) Ali, S.; Hassan, M.; Islam, A.; Ahmad, F. A Review of Methods Available to Estimate Solvent-Accessible Surface Areas of Soluble Proteins in the Folded and Unfolded States. *Curr. Protein Pept. Sci.* **2014**, *15*, 456–476.

(59) Hanić, M.; Frederiksen, A.; Schuhmann, F.; Solov'yov, I. A. On the Energetic Differences of Avian Cryptochromes 4 from Selected Species. *Eur. Phys. J. D* **2022**, *76*, 198.

(60) Schuhmann, F.; Korol, V.; Solov'yov, I. A. Introducing Pep McConst—A User-Friendly Peptide Modeler for Biophysical Applications. *J. Comput. Chem.* **2021**, *42*, 572–580.

(61) Chen, R.; Weng, Z. A Novel Shape Complementarity Scoring Function for Protein–Protein Docking. *Proteins: Struct., Funct., Genet.* **2003**, *51*, 397–408.

(62) Pierce, B. G.; Hourai, Y.; Weng, Z. Accelerating Protein Docking in ZDOCK Using an Advanced 3D Convolution Library. *PLoS One* **2011**, *6*, 246577.

(63) Pierce, B. G.; Wiehe, K.; Hwang, H.; Kim, B. H.; Vreven, T.; Weng, Z. ZDOCK Server: Interactive Docking Prediction of Protein–Protein Complexes and Symmetric Multimers. *Bioinformatics* **2014**, *30*, 1771–1773.

(64) Phillips, J. C.; Braun, R.; Wang, W.; Gumbart, J.; Tajkhorshid, E.; Villa, E.; Chipot, C.; Skeel, R. D.; Kalé, L.; Schulten, K. Scalable Molecular Dynamics with NAMD. *J. Comput. Chem.* **2005**, *26*, 1781–1802.

(65) Pierce, B.; Tong, W.; Weng, Z. M-ZDOCK A Grid-Based Approach for C<sub>n</sub> Symmetric Multimer Docking. *Bioinformatics* **2005**, *21*, 1472–1478.

(66) Zhang, Y. I-TASSER Server for Protein 3D Structure Prediction. *BMC Bioinf.* **2008**, *9*, 40.

(67) Roy, A.; Kucukural, A.; Zhang, Y. I-TASSER: a unified platform for automated protein structure and function prediction. *Nat. Protoc.* **2010**, *5*, 725–738.

(68) Yang, J.; Yan, R.; Roy, A.; Xu, D.; Poisson, J.; Zhang, Y. The I-TASSER Suite: Protein Structure and Function Prediction. *Nat. Methods* **2014**, *12*, 7–8.

(69) Yang, J.; Zhang, Y. I-TASSER Server: New Development for Protein Structure and Function Predictions. *Nucleic Acids Res.* **2015**, *43*, 174–181.

(70) Phillips, J. C.; Hardy, D. J.; Maia, J. D. C.; Stone, J. E.; Ribeiro, J. V.; Bernardi, R. C.; Buch, R.; Fiorin, G.; Hénin, J.; Jiang, W.; et al. Scalable Molecular Dynamics on CPU and GPU Architectures with NAMD. *J. Chem. Phys.* **2020**, *153*, 044130.

(71) Korol, V.; Husen, P.; Sjulstok, E.; Nielsen, C.; Friis, I.; Frederiksen, A.; Salo, A. B.; Solov'yov, I. A. Introducing VIKING: A

Novel Online Platform for Multiscale Modeling. *ACS Omega* **2020**, *5*, 1254–1260.

(72) Best, R. B.; Zhu, X.; Shim, J.; Lopes, P. E. M.; Mittal, J.; Feig, M.; MacKerell, A. D. J. Optimization of the Additive CHARMM All-Atom Protein Force Field Targeting Improved Sampling of the Backbone  $\phi$ ,  $\psi$  and Sidechain  $\chi_1$  and  $\chi_2$  Dihedral Angles. *J. Chem. Theory Comput.* **2012**, *8*, 3257–3273.

(73) Mackerell, A. D.; Feig, M.; Brooks, C. L. Extending the treatment of backbone energetics in protein force fields: Limitations of gas-phase quantum mechanics in reproducing protein conformational distributions in molecular dynamics simulations. *J. Comput. Chem.* **2004**, *25*, 1400–1415.

(74) Lüdemann, G.; Solov'yov, I. A.; Kubař, T.; Elstner, M. Solvent Driving Force Ensures Fast Formation of a Persistent and Well-Separated Radical Pair in Plant Cryptochrome. *J. Am. Chem. Soc.* **2015**, *137*, 1147–1156.

(75) Solov'yov, I. A.; Domratcheva, T.; Schulten, K. Separation of Photo-Induced Radical Pair in Cryptochrome to a Functionally Critical Distance. *Sci. Rep.* **2014**, *4*, 3845.

(76) Sjulstok, E.; Olsen, J. M. H.; Solov'yov, I. A. Quantifying Electron Transfer Reactions in Biological Systems: What Interactions Play the Major Role? *Sci. Rep.* **2015**, *5*, 18446.

(77) Feller, S. E.; Zhang, Y.; Pastor, R. W.; Brooks, B. R. Constant Pressure Molecular Dynamics Simulation: The Langevin Piston Method. *J. Chem. Phys.* **1995**, *103*, 4613–4621.

(78) Jorgensen, W. L.; Chandrasekhar, J.; Madura, J. D.; Impey, R. W.; Klein, M. L. Comparison of Simple Potential Functions for Simulating Liquid Water. *J. Chem. Phys.* **1983**, *79*, 926–935.

(79) Humphrey, W.; Dalke, A.; Schulten, K. VMD: Visual Molecular Dynamics. *J. Mol. Graphics* **1996**, *14*, 33–38.

(80) Sousa, S. F.; Neves, R. P. P.; Waheed, S. O.; Fernandes, P. A.; Ramos, M. J. Structural and Mechanistic Aspects of S-S Bonds in the Thioredoxin-like Family of Proteins. *Biol. Chem.* **2019**, *400*, 575–587.

(81) Kabsch, W. A discussion of the solution for the best rotation to relate two sets of vectors. *Acta Crystallogr., Sect. A: Cryst. Phys., Diffraction, Gen. Crystallogr.* **1978**, *34*, 827–828.

(82) Prinz, W. A.; Åslund, F.; Holmgren, A.; Beckwith, J. The Role of the Thioredoxin and Glutaredoxin Pathways in Reducing Protein Disulfide Bonds in the *Escherichia coli* Cytoplasm. *J. Biol. Chem.* **1997**, *272*, 15661–15667.

(83) Jakob, U.; Eser, M.; Bardwell, J. C. A. Redox Switch of Hsp33 Has a Novel Zinc-Binding Motif. *J. Biol. Chem.* **2000**, *275*, 38302–38310.

(84) Choi, H.; Kim, S.; Mukhopadhyay, P.; Cho, S.; Woo, J.; Storz, G.; Ryu, S. Structural Basis of the Redox Switch in the OxyR Transcription Factor. *Cell* **2001**, *105*, 103–113.

(85) Wang, Q.; Lin, C. Mechanisms of Cryptochrome-Mediated Photoresponses in Plants. *Annu. Rev. Plant Biol.* **2020**, *71*, 103–129.

(86) Schmalen, I.; Reischl, S.; Wallach, T.; Klemz, R.; Grudziecki, A.; Prabu, J. R.; Benda, C.; Kramer, A.; Wolf, E. Interaction of Circadian Clock Proteins CRY1 and PER2 Is Modulated by Zinc Binding and Disulfide Bond Formation. *Cell* **2014**, *157*, 1203–1215.